

Absorbing aerosol-induced change in the early monsoon Arabian Sea low-level jet: Modeled transfer from anomalous heating to nondivergent kinetic energy

Andrew C. Martin,^{1,2} T. N. Krishnamurti,¹ and William K. M. Lau³

Received 6 March 2013; revised 1 November 2013; accepted 4 November 2013; published 27 November 2013.

[1] This study examines the impact of anomalous differential generation of available potential energy by absorbing aerosols on the transition and early active phases of the South Asian summer monsoon. Aerosol direct and indirect radiative forcings can modify tropospheric temperature profiles through direct absorption, scattering, and extended cloud lifetimes. Recent studies have suggested that over monthly and seasonal time scales, these effects can lead to modified flow and rainfall regimes in the South Asian monsoon region. Of special interest is the covariance of heating and temperature prior to active monsoon onset. It can be shown that anomalous generation of available potential energy due to absorption of shortwave radiation by aerosols can impact the cascade of energy from the local Hadley circulation to the monsoon nondivergent flow. In order to quantify the potential impact of aerosol radiative forcing and the resulting changes in monsoon onset timing and intensity, an ensemble of Weather Research and Forecasting with Chemistry regional weather and chemistry model forecasts are created for the South Asian summer monsoon region during May, June, and July. The forecasts including shortwave absorption by aerosol are compared to control forecasts in which aerosols only scatter shortwave radiation. The evolution of irrotational and nondivergent kinetic energy, generation of available potential energy and rainfall are presented. It is found that the ensemble with aerosol shortwave absorption contains on average a more intense dynamical onset over South India which is statistically significant compared to the ensemble variability. The more intense monsoon onset is related to a more intense Arabian Sea low-level jet. In the ensemble with shortwave absorption by aerosol, the early season monsoon rainfall is diminished over South India and enhanced over the Northeastern Indian states.

Citation: Martin, A. C., T. N. Krishnamurti, and W. K. M. Lau (2013), Absorbing aerosol-induced change in the early monsoon Arabian Sea low-level jet: Modeled transfer from anomalous heating to nondivergent kinetic energy, *J. Geophys. Res. Atmos.*, *118*, 12,566–12,576, doi:10.1002/2013JD019808.

1. Introduction

[2] Atmospheric aerosols and their impact on the South Asian monsoon have become a growing subject of research in the past decade. Multiple year experiments such as the Joint Aerosol Monsoon Experiment [Lau *et al.*, 2008], and the Indian Ocean Experiment [Lelieveld *et al.*, 2001] have focused on the role aerosols play in modifying monsoon hydrology. The reasons for this scrutiny can be found in

two concurrent trends. The first is an observed trend in the regional hydrology. The countries of South Asia receive 75 to 90% of their annual rainfall from the summer phase of the monsoon. Studies by Fan *et al.* [2010] and Ramanathan and Ramana [2005] have indicated that monsoon rainfall has been diminishing since 1950. During this same time period, drought frequency by decade in South Asia has increased [Ramanathan *et al.*, 2005]. More than 20% of the Earth's population lives in the countries of South Asia [US Census Bureau, 2011]. The residents of these countries rely on monsoon rainfall not only for agriculture but have intertwined their cultures with the seasonal cycle of the monsoon.

[3] The second trend is more closely related to the rapid industrialization which some South Asian countries have experienced since the latter twentieth century. Anthropogenic emission of aerosol in the countries of India, Nepal, and Bangladesh now rivals or surpasses the levels seen in the United States and Western Europe [Ramanathan and Ramana, 2005]. The accelerating pace of emission has

¹Department of Earth, Ocean and Atmospheric Science, Florida State University, Tallahassee, Florida, USA.

²Department of Chemistry and Biochemistry, University of California, San Diego, California, USA.

³NASA Goddard Space Flight Center, Greenbelt, Maryland, USA.

Corresponding author: A. Martin, Department of Chemistry and Biochemistry, University of California, San Diego, 2108 Urey Hall, 9500 Gilman Dr., MC 0332, La Jolla, CA 92093-0332, USA. (mc@ucsd.edu)

contributed to more aerosol loading over the region. A study by Wang *et al.* [2009b] found that clear sky visibility over South Asia has decreased faster than in any other region since 1973.

[4] The method by which heavy aerosol loads in the South Asian troposphere could cause a change in summer monsoon rainfall is not fully established. The theories which have been proposed thus far can be divided by their two primary forcing mechanisms. Chung and Ramanathan [2006] proposed that a meridionally uneven aerosol load could lead to differential cooling of the sea surface over the Indian Ocean through reduction of solar insolation at the surface. The positive meridional surface temperature gradient which exists between the equatorial ocean and Asia is the primary driving force behind the northward migration of the local Hadley circulation in May, June, and July and thus behind the northward advance of monsoon rainfall during this period. The “differential sea surface cooling hypothesis” holds that cooling of the sea surface by aerosols in the northern Indian Ocean has masked the late 20th century and early 21st century warming trend seen in other oceanic basins. The equatorial Indian Ocean surface, by contrast, has warmed much like other basins over the past five to six decades. The net effect is a decreased meridional sea surface temperature gradient and a less intense monsoon.

[5] An alternate theory for aerosol-monsoon interaction is proposed by Lau *et al.* [2006]. The “elevated heat pump” (EHP) hypothesis relies on the finding that midlayer solar absorption by aerosols is especially high in the springtime over the Indo-Gangetic plain (IGP) and Himalayan foothills (HF) [e.g., Bollasina *et al.*, 2008; Ramanathan *et al.*, 2007]. During this time, the local Hadley circulation is advancing toward this area, and midtropospheric heating rates are elevated due to convection nearby. The anomalous heating due to aerosol absorption accelerates the advance of the Hadley cell in the late spring (May and early June), which leads to more vigorous meridional flow, more moisture convergence over continental India and more monsoon rainfall in the orographically forced areas of South Asia. Lau *et al.* [2006] also found in their numerical experiments that rainfall diminished over southern and central India during the active summer monsoon season (June–July–August–September).

[6] The mechanism which causes a reduction in lower India rainfall is not proposed by Lau *et al.* [2006]. However, since the rising branch of the meridional circulation has migrated north of this location by the onset of the active South Asian summer monsoon, it is likely that there is a separate fluid-dynamic explanation. It is also clear from Lau *et al.* [2006] and others [e.g., Wu and Zhang, 1998; Wu *et al.*, 1997; Li and Yanai, 1996] that the nature of the monsoon-aerosol interaction takes on a different character near monsoon onset than it does during the late season.

[7] The goal of this study is to fully describe the fluid dynamics behind the elevated heat pump mechanism of aerosol-monsoon interaction and to show that the aerosol absorption has consequences on flow features beyond the primary rising branch of the Hadley cell. It will become apparent that one feature which is highly sensitive to springtime aerosol absorption over the IGP and HF is the Arabian Sea low-level jet (AS LLJ). The onset timing and intensity of the South Asian summer monsoon, as well as the rainfall over southern India is very sensitive to the location and

intensity of this jet. Therefore, the response of rainfall and winds at onset to anomalous heating by absorbing aerosols is also investigated.

[8] To calculate a response to IGP/HF aerosol absorption in the Arabian Sea low-level jet, an ensemble of with and without forecasts have been made using the Weather Research and Forecasting with Chemistry (WRF/CHEM) model. The analysis of these forecasts is presented in the remaining sections. The rest of this article is organized as follows: The fluid dynamic theory which describes energy transfer from aerosol absorption to AS LLJ kinetic energy is given in section 2. Section 3 presents the experiment methodology, including model and ensemble description, initial and boundary conditions, and postprocessing. Section 4 presents modeled results regarding energy exchanges and the resulting characteristics of the AS LLJ near summer monsoon onset. A discussion of results is given in section 5.

2. Background and Theory

2.1. Aerosol Heating

[9] As was mentioned in the previous section, aerosols can impact both radiative transfer and precipitation processes. The radiative transfer impacts can be broken into aerosol direct radiative effects and the first aerosol indirect effect which is also called the Twomey effect. The impact on precipitation is the result of a set of aerosol-cloud microphysics interactions known as the second aerosol indirect effects. The aerosol direct effects can be further broken into the radiative forcing due to aerosol scattering and aerosol absorption. Nearly all aerosol species are effective at scattering shortwave radiation. A few also absorb shortwave radiation. Other species (such as dust) absorb radiation in the thermal wavelengths. The net direct effect on atmospheric radiative transfer due to aerosols depends on which species are present in which layers, the vertical location of clouds relative to the aerosol and on the surface temperature, emissivity, and reflectivity. For a good discussion on aerosols and single-column radiative transfer, see Lacis and Mischenko [1995].

[10] Aerosols can also act as cloud condensation nuclei (CCN). Twomey [1977] was the first to describe the impact that this behavior has on atmospheric radiative transfer. More CCN in a cloudy environment leads to cloud droplets with smaller effective radius. Effective radius has a significant impact on the reflectivity of a cloud, especially in the ultraviolet, visible and near-infrared wavelengths. Therefore, the aerosol first indirect effect has an impact on radiative transfer similar to the scattering portion of the aerosol direct effects. On average, more shortwave radiation is reflected away from the Earth’s surface when clouds contain a high concentration of CCN. The change in vertical radiative flux convergence leads to cooling at the surface and at the top of the atmosphere. The reader is directed to Ramanathan and Carmichael [2008] for a qualitative description of the average radiative forcing which results from the aerosol direct effects and the first aerosol indirect effect. Assuming clear sky conditions and the presence of an absorbing aerosol species at some level in the troposphere, the net effect of the absorbing direct effect will be to cool the surface, but to warm the troposphere and the top of the

atmosphere. The second aerosol indirect effects have been shown to extend cloud lifetimes, and change the organization of convection at small scales [Freud *et al.*, 2005]. If cloud lifetimes are extended by the presence of aerosol, this can provide additional tropospheric heating through absorption and reemission of longwave radiation by the clouds over time. The magnitude of this additional longwave heating will increase with cloud altitude.

[11] The potential for anomalous tropospheric heating over the IGP/HF by aerosol has been well established by previous authors. The region was shown by Ramanathan *et al.* [2007] to contain very high concentration of black carbon aerosol. Black carbon is a very efficient absorber of shortwave radiation. In addition to black carbon, high concentrations of dust are often found over the IGP, the Arabian Sea, and the nearby desert regions. Dust weakly absorbs shortwave radiation, but when present in large quantities, the effect can be large total column absorption. Krishnamurti *et al.* [2009] found that aerosol indirect effects over the Arabian Sea could lead to anomalous heating and altered local circulation in a modeled atmosphere. The question which will be addressed in the next section is, How can heating through aerosol absorption impact the monsoon flow?

2.2. Fluid Dynamics of the Monsoon

[12] The mathematical framework used to illustrate the impact of aerosol heating on monsoon flow will be the “psi-chi” interaction theory of Krishnamurti and Ramanathan [1982, hereafter KR82]. The framework is constructed by partition of the horizontal flow into nondivergent (v_ψ) and irrotational (v_χ) components. The nondivergent component represents the sheared and curved flow. It is expressed in terms of the stream function (ψ) as

$$v_\psi = \mathbf{k} \times \nabla \psi. \quad (1)$$

The irrotational component represents the divergent flow contained in thermally driven overturning circulations, it is expressed in terms of the velocity potential (χ) as

$$v_\chi = -\nabla \chi. \quad (2)$$

By casting the primitive vorticity and divergence equations in terms of ψ and χ , the equation for the irrotational flow kinetic energy can be found by the product $\chi \frac{\partial D}{\partial t}$, while the equation for the nondivergent flow kinetic energy can be found by the product $\psi \frac{\partial \zeta}{\partial t}$. In addition to these two equations, a third can be found by combining the first law of thermodynamics with the equation of state for dry air. This third equation is that for available potential energy (P_a), which is called “internal plus potential energy” in KR82. By integrating over a closed domain, the domain-total available potential energy ($\overline{P_a}$), irrotational kinetic energy ($\overline{K_\chi}$) and nondivergent kinetic energy ($\overline{K_\psi}$) are given by

$$\frac{\partial \overline{P_a}}{\partial t} = \overline{\chi \nabla^2 \phi} + \overline{G_p} + \overline{D_p} + B_p, \quad (3)$$

$$\begin{aligned} \frac{\partial \overline{K_\chi}}{\partial t} = & -\overline{\chi \nabla^2 \phi} - \overline{(f + \nabla^2 \psi)(\nabla \psi \cdot \nabla \chi)} - \frac{\overline{\nabla^2 \chi (\nabla^2 \psi)}}{2} \\ & - \omega J \left(\psi, \frac{\partial \chi}{\partial p} \right) + \overline{D_\chi} + B_\chi \quad \text{and} \end{aligned} \quad (4)$$

$$\begin{aligned} \frac{\partial \overline{K_\psi}}{\partial t} = & \overline{(f + \nabla^2 \psi)(\nabla \psi \cdot \nabla \chi)} + \frac{\overline{\nabla^2 \chi (\nabla^2 \psi)}}{2} \\ & + \omega J \left(\psi, \frac{\partial \chi}{\partial p} \right) + \overline{D_\psi} + B_\psi. \end{aligned} \quad (5)$$

[13] In the above equations, ω is the vertical motion across isobaric surfaces, $D_{p,\chi,\psi}$ is the dissipation of kinetic or potential energy, $B_{p,\chi,\psi}$ is the flux of energy across the domain boundary, G_p is the generation of available potential energy and $J()$ is the Jacobian operator.

[14] The generation of P_a can be expressed as

$$\overline{G_p} = \frac{1}{g} \int_{ps}^{pt} \frac{c_p Q' T'}{\overline{T}} dP, \quad (6)$$

[15] where Q' is the local heating anomaly, T' is the local temperature anomaly \overline{T} is the layer average temperature and P is the pressure. It is expected that absorption of shortwave radiation by aerosols can provide the local heating anomaly, and that this heating anomaly can become especially large over the IGP/HF in the springtime before monsoon onset.

[16] There are three primary lessons contained in equations (3)–(5) which are pertinent to the transfer of potential energy which is generated inside the monsoon domain to the kinetic energy of the nondivergent flow. The first lesson is that the available potential energy can only be converted to and from *irrotational* kinetic energy. The first term appearing in the right hand side of equations (3) and (4) represents the exchange of energy between P_a and K_χ . We will refer to this term hereafter as the thermal efficiency term, $\langle P_a, K_\chi \rangle$. Rising motion in relatively warm columns converts P_a to K_χ . This can be illustrated by rearranging $\langle P_a, K_\chi \rangle$ using the mass continuity equation, the first law of thermodynamics and the ideal gas law,

$$\langle P_a, K_\chi \rangle = -\overline{\chi \nabla^2 \phi} = -\frac{\overline{R \omega' T'}}{P}. \quad (7)$$

[17] The term $\langle P_a, K_\chi \rangle$ along with $\overline{G_p}$ and the tropospheric heating anomaly over the IGP/HF form the mathematical expression of the EHP hypothesis.

[18] The second lesson is that, neglecting boundary fluxes, the nondivergent flow can only gain energy at the expense of the irrotational flow and vice versa. This is seen in the “psi-chi exchanges”, $\overline{(f + \nabla^2 \psi)(\nabla^2 \chi \cdot \nabla \chi)}$, $\frac{\overline{\nabla^2 \chi (\nabla^2 \psi)}}{2}$, and $\omega J \left(\psi, \frac{\partial \chi}{\partial p} \right)$. Of these terms, the first has been found to be the most important for the increase of nondivergent kinetic energy during the summer monsoon period in South Asia [KR82, Krishnamurti *et al.*, 1998]. This term will be referred to as the psi-chi exchange, which is expressed as $\langle K_\chi, K_\psi \rangle \simeq \overline{(f + \nabla^2 \psi)(\nabla^2 \chi \cdot \nabla \chi)}$.

[19] The third lesson comes from the way that the horizontal flow components are defined in terms of the velocity potential and stream function. Because of the form of v_χ (see equation (2)), a local increase in K_χ amounts to the formation of a peak or valley in the velocity potential field. The velocity potential is a continuous function, therefore the gradient, $\nabla \chi$ will respond to a change in K_χ nonlocally. The dot product in the psi-chi exchange then allows for the possibility that an increase in available potential energy can cascade to the nondivergent kinetic energy at a different location.

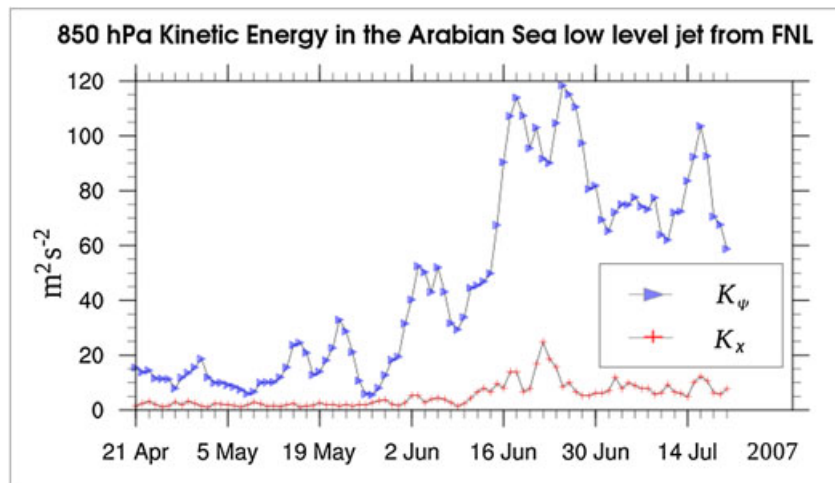


Figure 1. Area mean 850 hPa K_χ and K_ψ from FNL analysis in the area enclosed between 2°N to 10°N and 45°E to 77°E during the premonsoon and early active season, 2007.

2.3. Impact on Onset and the Arabian Sea Low-Level Jet

[20] A major finding of KR82 has to do with the relationship of the AS LLJ and the start of heavy summer monsoon rain. The authors found that the mean horizontal kinetic energy in the region near the jet increases explosively just before daily rains commence over central India. Nearly all of the increase is contained in the nondivergent kinetic energy. Figure 1 depicts the area mean irrotational and nondivergent kinetic energy at 850 hPa in the vicinity of the AS LLJ from the National Centers for Environmental Prediction (NCEP) Global Forecast System final analysis (FNL) for the summer monsoon season of 2007. Note that K_ψ rapidly doubles near 15 June 2007, while K_χ stays nearly constant. After this date, the value of K_ψ stays at a higher plateau.

[21] The increase of nondivergent kinetic energy over the jet region also corresponds to the AS LLJ extending eastward from the Somali coast. On average, westerlies with 15 m s^{-1} or greater speed reach the west coast of Kerala, India near the first week of June. Several authors have tied the onset of the summer monsoon to robust low-level westerlies over Kerala [e.g., Wang *et al.*, 2009a; Fasullo and Webster, 2003; Ananthakrishnan and Soman, 1988]. The event near 15 June in Figure 1 can be thought of as the AS LLJ reaching “dynamical maturity”. The nondivergent kinetic energy experiences a quasi-permanent state change which is fed primarily by energy from the local Hadley circulation through the psi-chi exchange. The timing of this state change, and the resulting moisture transport and cyclonic shear over southwestern India suggest that it is nontrivially related to the onset of the South Asian summer monsoon.

3. Data and Methods

[22] The model used to simulate the monsoon onset period is the WRF/CHEM regional weather chemistry and transport model version 3.3.1 [Grell *et al.*, 2005]. An ensemble of with shortwave absorbing aerosol (CHEM) and without shortwave absorbing aerosol (NOABS) forecasts have been run. CHEM forecasts include interactive aerosol mass and

optical properties, as well as aerosol-cloud microphysics interaction. In NOABS forecasts, all of the above aerosol processes are active, except that the complex index of refraction used by the radiation code to calculate absorption in the ultraviolet and visible wavelengths is set to zero for all aerosol species. Aerosol chemistry, including nucleation, growth, coagulation, and removal is computed by the Modal Aerosol Dynamics Model for Europe/Secondary Organic Aerosol Model [Ackermann *et al.*, 1998]. Emissions come from the Global Ozone Chemistry Aerosol Radiation and Transport climatology emissions data set for natural and primary anthropogenic aerosol emissions [Ginoux *et al.*, 2001] and the REanalysis of the TROposphere (RETRO) global emissions data set for gaseous precursor emissions [Bolscher *et al.*, 2007]. Biomass burning emissions are estimated according to the data contained in the Moderate Resolution Imaging Spectroradiometer (MODIS) daily fire detection product [Justice *et al.*, 2002]. Global emissions are prepared for the WRF/CHEM domain by the preprocessor described in [Freitas *et al.*, 2011].

[23] CCN activation is calculated by the method of Abdul-Razzak and Ghan [2000]. Cloud droplet size distribution truncation is found by the method presented in Liu and Daum [2004]. These, in turn impact the autoconversion process in the Lin-Purdue microphysics model [Lin *et al.*, 1983; Rutledge and Hobbs, 1984]. Shortwave radiative transfer is calculated by the NASA Goddard Space Flight Center CLIRAD radiative transfer band model (Goddard scheme) [Chou and Suarez, 1999]. The Goddard scheme calculates scattering and absorption by aerosol. Longwave radiative transfer is calculated by the updated Rapid Radiative Transfer Model (RRTMG) [Clough *et al.*, 2005]. RRTMG calculates the layer aerosol longwave absorption according to bulk aerosol optical depth. The above physics parameterizations allow scattering, absorption and first and second (warm rain only) aerosol indirect effect to be calculated in both the CHEM and NOABS forecasts, while shortwave aerosol absorption is only present in the CHEM forecasts.

[24] The WRF/CHEM domain has a horizontal resolution of 50 km and extends meridionally from 29° south latitude to 53° north latitude, or from the southern midlatitudes to

southern central Siberia. The zonal extent of the domain is from 25° east longitude to 139° east longitude, or from central Africa to the Philippine Sea at 10° North. The model is divided into 32 vertical levels on the WRF hybrid surface following coordinate [Skamarock et al., 2008]. This very large domain allows for the removal of boundary fluxes (i.e., B_χ and B_ψ in equations (4) and (5)) to well beyond the region containing the IGP/HF and AS LLJ. Each forecast is run continuously without adjustment for 91 days from 21 April at 0000 UTC to 20 July at 0000 UTC. This allows the relatively small perturbations to the atmospheric radiation budget in the CHEM forecasts to build thermodynamic anomalies over South Asia for many weeks, as can happen in the real premonsoon environment.

[25] An ensemble of 10 forecasts has been run using both the CHEM and NOABS configurations. The ensemble members differ only in their initial conditions. The boundary conditions and prescribed sea surface temperature (SST) are shared among all ensemble members. Initial and boundary conditions come from FNL; SST comes from the NCEP real-time sea surface analysis (RTG). Both FNL and RTG are from the year 2007. This season was chosen because in 2007, all-India monsoon rainfall was within its normal range, the El-Niño Southern Oscillation was in its neutral phase, and the Indian Ocean Dipole was neutral as well [Shaik and Cleland, 2008].

[26] The motivation for creating an ensemble of forecasts, rather than a single realization, was so that the significance of aerosol impact on the psi-chi energy exchanges could be estimated relative to Gaussian climate variability in the premonsoon atmospheric state. The FNL initial condition was perturbed according to the Monte Carlo method of Mullen and Baumhelfner [1993]. To estimate the Gaussian range of climate variability in the initial state, 30 years of NCEP / National Center for Atmospheric Research (NCAR) Reanalysis 1 data [Kalnay et al., 1996] for the three-dimensional zonal wind (u), meridional wind (v), temperature (T), and water vapor mixing ratio (q_v) were used.

[27] Forecast histories were postprocessed so that the generation of P_a , thermal efficiency, and psi-chi exchange could be compared CHEM to NOABS and between members of the same ensemble. The forecast u and v were transformed to ψ and χ using spherical harmonic transformation. Vertical integrals were performed in model native coordinates, but the transfers $\langle P_a, K_\chi \rangle$ and $\langle K_\chi, K_\psi \rangle$ were calculated on isobaric surfaces after vertical interpolation from the model native coordinate.

[28] Onset was found through the method suggested by Fasullo and Webster [2003 - hereafter FW03]. According to the authors, onset of the summer monsoon over a given region of South Asia can be found by examining the field of vertically integrated moisture transport (V). In this study, we were interested in onset over Kerala, which is the most commonly used date for onset of the South Asian summer monsoon by the India Meteorological Department. Since onset over Kerala corresponds closely to the arrival of a deep layer of low-level westerly winds, this study used the following definition of V ,

$$V = \frac{1}{g} \int_{P_s}^{300\text{hPa}} uq_v dP. \quad (8)$$

[29] Note that in equation (8), only the zonal component of horizontal wind appears in the vertical integral, while FW03 use the full horizontal wind vector. FW03 do not propose a threshold in V for declaring onset. Through examining both NCAR/NCEP R1 data and the forecast ensembles, it was found that the first peak following explosive growth in the time series of area mean AS LLJ K_ψ occurred within 1 to 2 days of area mean V for Kerala increasing beyond 6 kg m⁻² m s⁻¹. In the results to follow, when this threshold is crossed for a given ensemble member, dynamic onset over Kerala (DOK) has been reached. Area mean K_ψ in the AS LLJ ($\overline{K_\psi}$) was found by taking the average between 2°N to 10°N and 45°E to 77°E. Vertically integrated moisture transport over Kerala (V_K) was found by the area mean V between 8°N to 12°N and 75°E to 80°E.

4. Results

4.1. Energy Exchanges

[30] The ensemble forecast experiment was designed so that the CHEM forecasts would have strong aerosol absorption in black carbon and dust rich regions, while the NOABS forecasts would not. The model's internal chemistry and three-dimensional transport determine where these aerosol species collect during the premonsoon period. Forecast verification of aerosol optical and mass fields was performed using MODIS and the Aerosol Robotic Network.

[31] Figure 2 shows the mean fractional bias in the CHEM ensemble aerosol optical depth at 550 nm (AOD_{550}) compared to MODIS Level 3 daily AOD_{550} from June 2007. It should be noted that the model variable in this comparison is output daily at 1130 local time (0600 UTC), which is 1 h later than the equator crossing time of the Terra spacecraft. Since the Aqua spacecraft crosses much later in the afternoon, MODIS AOD_{550} from Aqua was not used in this comparison. The model consistently overestimates AOD_{550} throughout this part of the domain, but over most of the IGP and toward the Himalayan foothills, the bias in CHEM ensemble AOD is only about 25%. The overestimate is much higher—as much as 60%—in other places. As will be shown later, the IGP and HF are the most important areas for the anomalous shortwave generation of available potential energy. While aerosol optical depths are high, the model does produce realistic values of radiative forcing over Northern India. Table 1 contains the CHEM and NOABS ensemble mean “apparent” atmospheric radiative forcing due to aerosols during the month of June over the IGP and HF and compares it to the values found in several previous studies from the same region at various times of the year. A third ensemble of simulations without aerosol emissions or aerosol and gaseous chemistry (ARW) was run in tandem with CHEM and NOABS. The apparent atmospheric forcing by aerosols was found by taking the column-integral

$$\Delta F' = \frac{1}{g} \int_{P_s}^{P_t} c_p (Q_{\text{CHEM,NOABS}} - Q_{\text{ARW}}) dP. \quad (9)$$

[32] Where Q_{CHEM} , Q_{NOABS} , Q_{ARW} are the values of diabatic heating simulated by the radiative transfer model in the CHEM, NOABS, ARW ensembles, respectively. The calculation is performed using the heating from the shortwave radiation model only and the heating from both longwave

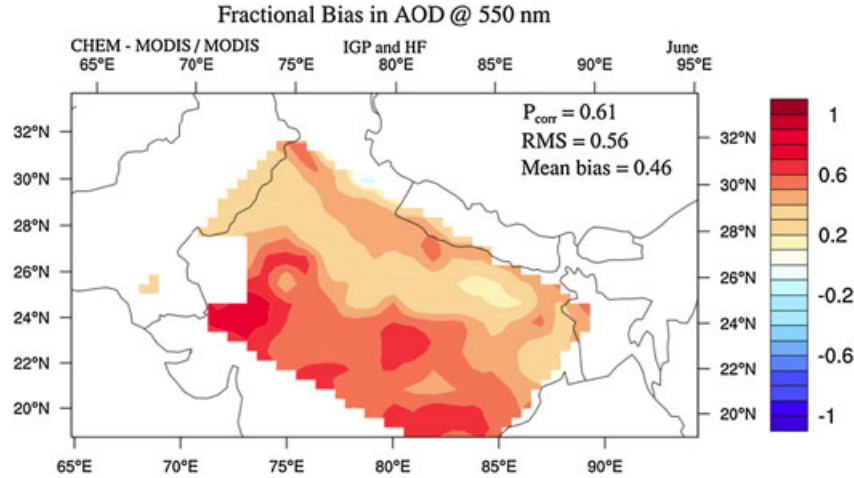


Figure 2. Fractional ensemble-mean bias in CHEM daily AOD_{550} compared to the same parameter from MODIS-Terra L3 Aerosol product for June 2007. Also shown are the mean pattern correlation (P_{corr}), root-mean-square error (RMS) and mean bias.

and shortwave models (“Total”). Diabatic heating is calculated by the radiative transfer models according to

$$Q = \frac{g}{c_p} \frac{d(F_{\downarrow} - F_{\uparrow})}{dP}. \quad (10)$$

[33] By substituting equation (10) into equation (9), one can approximate the total atmospheric forcing by

$$\Delta F' = \Delta(F_{\downarrow} - F_{\uparrow})|_{TOA} - \Delta(F_{\downarrow} - F_{\uparrow})|_{sfc}, \quad (11)$$

[34] if the atmosphere is considered a uniform slab between the top of the atmosphere (TOA) and the surface (sfc). The values reported from previous studies in Table 1 were found by applying equation (11). The apparent atmospheric forcing by aerosols in the CHEM ensemble is positive (net warming of the atmosphere) and similar in magnitude to the values reported by the other authors. The apparent atmospheric forcing by aerosols in the NOAB ensemble is weakly negative/positive for the shortwave/total mean. The difference between the two ensembles is that shortwave absorption by aerosols is active in the CHEM ensemble while it is not in NOABS. This analysis shows that the atmospheric diabatic heating by aerosols is realistic in the CHEM ensemble for the northern Indian region during the preonset and early active period while it is not realistic in the NOABS ensemble.

[35] The maxima in shortwave aerosol absorption occurs over the IGP and over the northern Bay of Bengal (BOB). This absorption creates tropospheric heating and generates available potential energy. Figures 3–6 show energy

Table 1. Apparent Radiative Forcing (Wm^{-2}) of the Atmospheric Column by Aerosols Over South Asia^a

Source	Shortwave	Total
CHEM - ARW (This Study)	62.1	56.3
NOABS - ARW (This Study)	-3.73	1.32
Ramanathan et al. [2007]		71 +/- 26
Vinoj et al. [2004]		0.2 - 20.5
Babu et al. [2002]		28

^aThe quoted value from Ramanathan et al. [2007] is the authors’ report of local values for Megacity “ABC Hotspots”.

exchange terms which were introduced in section 2. While equations (3)–(5) contain domain averages, we will present the local values of G_p , $\langle P_a, K_{\chi} \rangle$ and $\langle K_{\chi}, K_{\psi} \rangle$ in the figures to come. This is done to illustrate the spatial patterns by which energy cascades from available potential to kinetic energy of the AS LLJ.

[36] Figure 3 depicts the ensemble mean difference (CHEM-NOABS) G_p by total radiative heating (longwave plus shortwave) over the 21 days prior to DOK. There are two primary maxima in total G_p in the South Asian region. One is located over the eastern IGP and the northern BOB, while the other is located over the Arabian Sea. Generation of P_a through shortwave radiational heating dominates both regions. The vertical and spectral nature of G_p over the IGP are shown in more detail in the next figure.

[37] Figure 4 shows the evolution of the vertical profile of the ensemble mean difference (CHEM-NOABS) in area

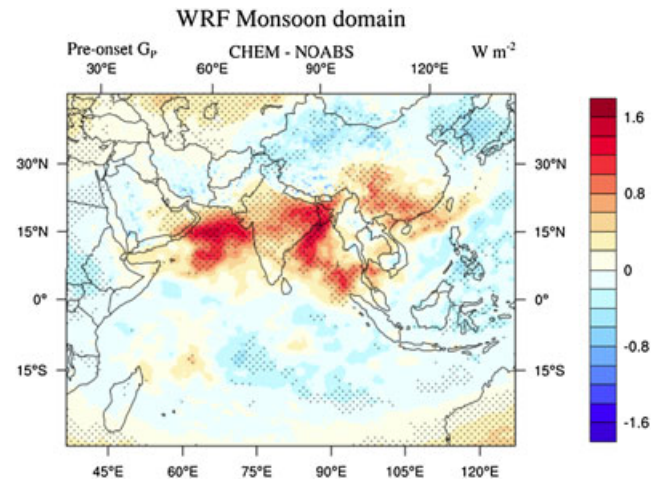


Figure 3. Ensemble mean difference in total G_p by model radiative transfer. The mean difference (CHEM-NOABS) for the 21 days prior to DOK is shaded. Areas for which the difference is significant according to the intraensemble t score are stippled.

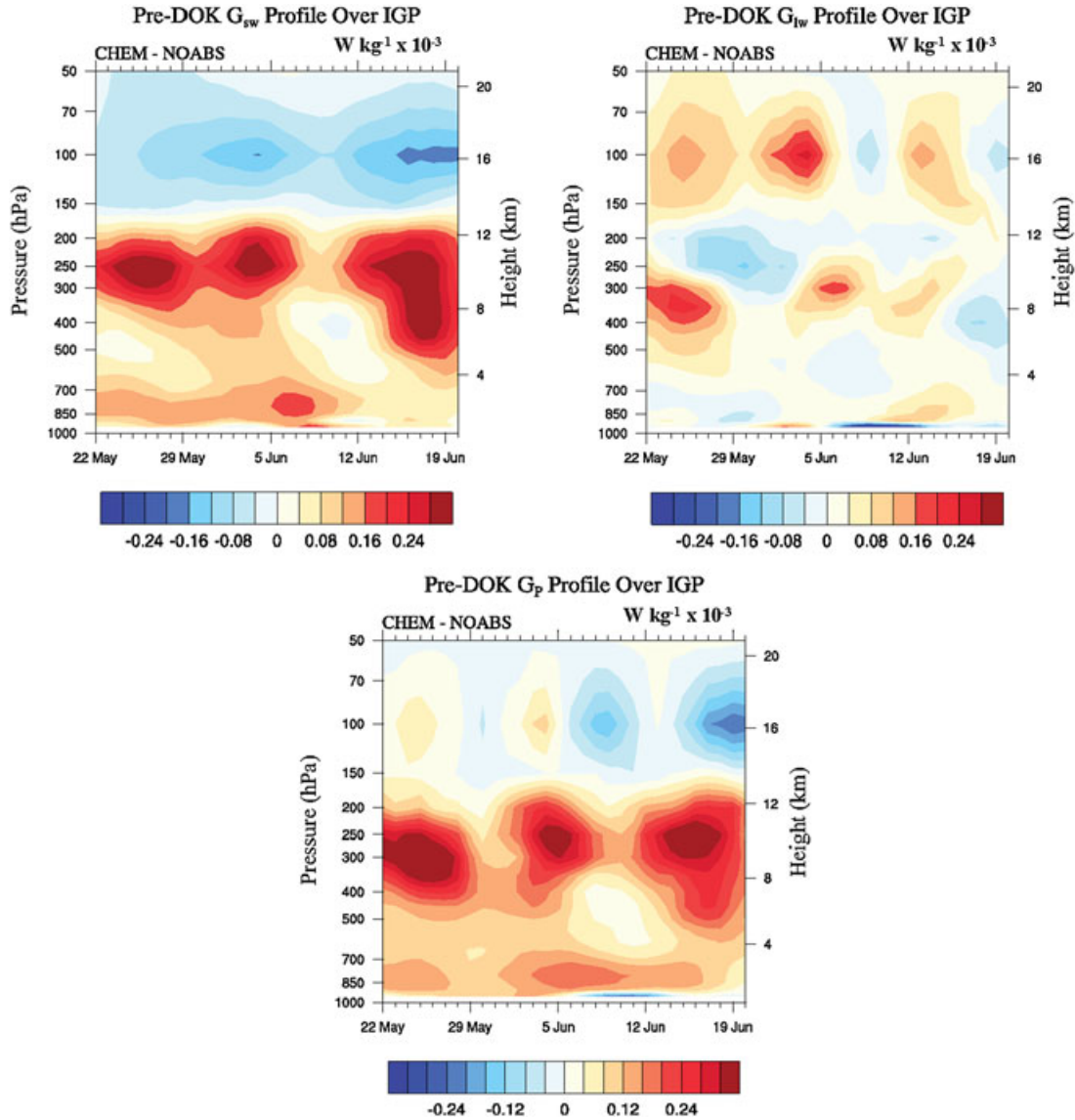


Figure 4. The Temporal evolution of the vertical profile of the components of G_p over the Eastern IGP maxima. Area means are enclosed by 7°N to 14°N and 60°E to 68°E . Clockwise from Top-left are G_{sw} , G_{lw} , and G_p .

average G_p over the Eastern IGP maxima with time, broken into its shortwave and longwave components. Over the IGP, The profile of generation of P_a stays fairly constant with time. There are two primary layers for which there is much greater G_p in the CHEM ensemble than in NOABS. There is an upper tropospheric layer located between 10 and 12 km altitude and a lower tropospheric layer located around 2 km. These correspond roughly to the mean vertical locations of the dust layer (upper) and industrial aerosol layer (lower) above the model springtime IGP. The figure shows that in these two vertical layers, generation of APE by shortwave radiative transfer processes in the CHEM ensemble is greater, and is the dominant radiative process. Since there is aerosol absorption in the CHEM ensemble only, this suggests that the anomalous generation of APE over the Eastern IGP is caused primarily due to absorption by black carbon (lower layer) and by dust (upper layer). There are some differences in the field of G_{lw} (top right). These

are due primarily to differences in the anomaly temperature field, especially at the surface and upper atmosphere (not depicted). Note that there is less stratospheric shortwave generation of available potential energy in the CHEM ensemble. This is likely due to reduced upwelling shortwave radiation because of the presence of tropospheric absorbing aerosols. Strong absorption causes diminished stratospheric heating through absorption of shortwave radiation by ozone.

[38] The excess generation of P_a in CHEM over the IGP during the period leading to onset has an impact on the thermal efficiency transfer. The difference (CHEM - NOABS) in 850 hPa ($\langle P_a, K_{\chi} \rangle$) for the 21 days prior to onset is shown in Figure 5. Locations for which the difference is statistically significant at the 95% or greater confidence interval are crosshatched. There is an excess of $\langle P_a, K_{\chi} \rangle$ in the CHEM forecasts over the eastern IGP and the Himalayan foothills. These are the same locations for which more available potential energy was generated in the CHEM forecasts.

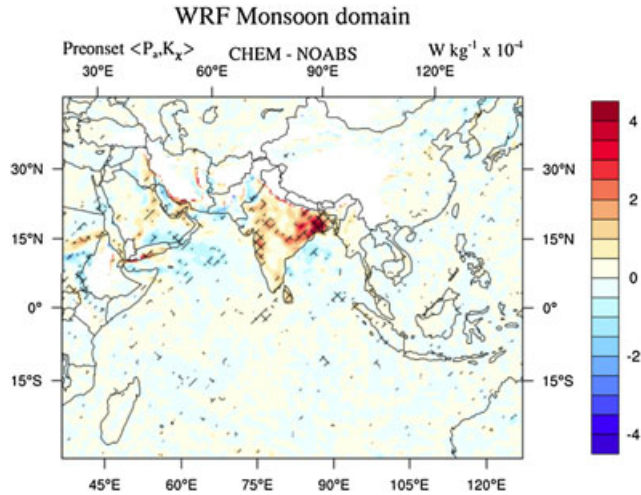


Figure 5. The ensemble mean difference (CHEM-NOABS) in 850 hPa $\langle P_a, K_\chi \rangle$ for the 21 days prior to onset. Cross-hatching indicates where the difference is significant at the 95% or greater confidence interval according to Student's t test.

This excess agrees well with the EHP hypothesis, whereby the action of a thermally direct vertical overturning circulation converts excess potential energy generated by absorbing aerosols to excess kinetic energy in this same location.

[39] The final step in transfer of energy from the aerosol radiative effects to the AS LLJ kinetic energy is the psi-chi transfer. The preonset difference (CHEM-NOABS, 21 days) in 850 hPa $\langle K_\chi, K_\psi \rangle$ is shown in Figure 6. Significance is displayed in the same manner as in Figure 5. Note that there is an excess in preonset transfer to the nondivergent kinetic energy over the central and eastern Arabian Sea in Figure 6, in a belt which corresponds to the mean location of the Arabian Sea low-level jet. The belt of enhanced 850 hPa $\langle K_\chi, K_\psi \rangle$ in CHEM stretches across southern India and intensifies and becomes statistically significant in the western Arabian Sea. To the west, near the tip of Somalia, there is a region for which the transfer is less in the CHEM forecasts. The pattern in Figure 6 has several important impacts on the regional low-level flow. Over the area in which the Jet forms, there is more energy transfer to nondivergent kinetic energy in the CHEM forecasts, except for over a small region near the Somali coast. This causes an eastward shift in the CHEM AS LLJ. Over the western BOB there is an enhancement in nondivergent kinetic energy just where a cyclonic turning in low-level flow forms during the mature summer monsoon. These features will be important to the analysis of the results regarding the jet location and intensity at onset, as well as the ensemble mean early season rainfall, which are presented next.

4.2. Intensity of the Jet at Onset

[40] From the V_K threshold presented above, DOK was found to occur in the FNL analyses on 18 June 2007. The date of DOK was also found for each ensemble member in NOABS and CHEM. For CHEM, DOK occurs on June 22 \pm 0.78 day. For NOABS, DOK occurs on June 22 \pm 1.08 day. The uncertainty quoted corresponds to the standard deviation of the date across the ensemble members. While it was

not postulated that the ensemble timing would change based on the anomalous aerosol forcing, it is noteworthy that the mean onset date from both ensembles is delayed slightly compared to the date of DOK in the analysis.

[41] After the onset date was identified, the mean non-divergent kinetic energy in the AS LLJ ($\overline{K_\psi}$) at onset was compared between CHEM and NOABS. This comparison is shown in Figure 7. The ensemble mean value of $\overline{K_\psi}$ for the 30 days prior to onset is displayed in the top. The NOABS time series is in blue, while the CHEM time series is in red. The bottom panel shows the difference (CHEM-NOABS) in the ensemble mean daily $\overline{K_\psi}$. By examining the time series, It is apparent that there is more nondivergent kinetic energy in the CHEM mean AS LLJ for 10 days prior to onset. This difference becomes significant prior to onset.

[42] Figure 8 shows the mean isotachs over the Arabian Sea at onset for both CHEM and NOABS. The reader should note that the jet in CHEM is more intense at onset by 5 m s⁻¹ and the CHEM jet extends further east than it does in NOABS. The eastward shift in the jet leads to greater moisture transport across southern India, but diminished moisture convergence in the CHEM ensemble forecasts over this region. As will be shown next, this has consequences for the early season rainfall in CHEM over southern India.

[43] The most pertinent way to measure the strength of the monsoon at onset is to measure rainfall for a short time period directly after onset. The comparison of post-onset average daily rainfall between the two ensembles is also displayed in Figure 8. The figure shows the difference (CHEM-NOABS) in the ensemble mean rainfall for 30 days after DOK over a portion of the model domain. The anomaly daily ensemble mean rainfall shows that the CHEM forecasts are slightly drier in southern India but much wetter in northeastern India and over the northern BOB during the early active season. The southern Indian states and the coast windward of the Ghats receive up to 2 mm day⁻¹ less rain in the CHEM forecasts, but some northern BOB coastal areas receive up to 8 mm day⁻¹ more rain during the same period in the CHEM ensemble. The drier south corresponds to a

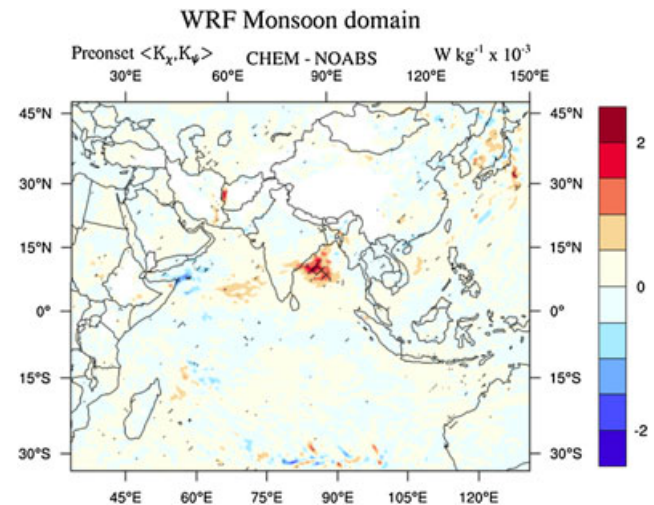


Figure 6. As in Figure 5, except that the field displayed is the difference in $\langle K_\chi, K_\psi \rangle$.

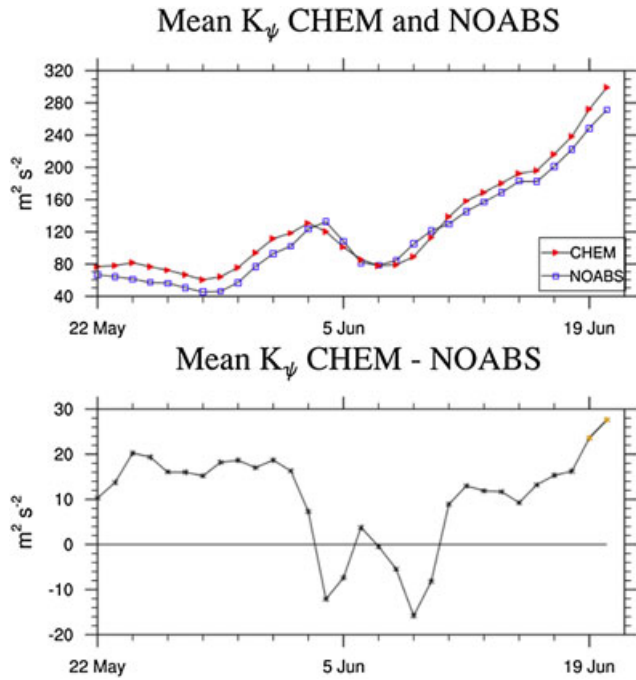


Figure 7. (a) The AS LLJ mean K_{ψ} for the 30 days prior to DOK. The CHEM ensemble mean is the red trace, The ARW ensemble mean is in blue. (b) The difference between CHEM and NOABS ensemble means. Points at which the difference is significant at 90% confidence or greater according to student's t test are highlighted in orange.

decrease in convergence of water vapor flux over the continent. This is a direct consequence of both the eastward extension of the AS LLJ and the deepening of 850 hPa low pressure over the AS in the CHEM forecast. The anomaly 850 hPa vectors during onset week show that the CHEM-NOABS low-level flow over southern India is offshore and divergent. The rainier northeast corresponds to an increase in 850 hPa curvature vorticity at the same time that convection and atmospheric moistening has commenced near onset (See

the anomaly 850 hPa flow vectors in Figure 8). Both of these features are driven by low-level dynamics and are the result of the anomalous pattern of kinetic energy transfer from the irrotational flow to the nondivergent flow. As shown in Figures 3–6, the low level transfer $\langle K_{\chi}, K_{\psi} \rangle$ is perturbed by midtropospheric heating over the IGP in the CHEM forecasts. Figure 8 shows the consequences that these anomalous energy transfers have on the low-level flow at onset and on the early active season rainfall.

5. Discussion

[44] Two ensembles of 90 day forecasts have been completed with and without shortwave absorption by aerosols using the WRF/CHEM weather chemistry and transport model. The domain and time period were chosen so that the forecasts simulated the premonsoon and onset period of the South Asian summer monsoon. The ensemble member initial conditions were perturbed to represent the Gaussian climate variability about a mean state which was chosen as the South Asian atmosphere and surface in 2007.

[45] After completion, the onset timing, rainfall, and intensity and location of the Arabian Sea low-level jet were compared between ensembles. No difference in onset timing between the CHEM and NOABS ensembles was found. It was found that the CHEM AS LLJ was more intense at onset than its NOABS counterpart by up to 5 m s^{-1} in the western Arabian Sea. In addition, the 20 m s^{-1} isotach reached the southwest Indian coast at onset in CHEM, but did not extend as far east in the NOABS forecasts.

[46] It was postulated in the theory section that the psi-chi framework would allow one to follow the cascade of energy from anomalous generation of P_a through the thermal efficiency exchange to the primary psi-chi exchange, and that the dot product in the primary psi-chi exchange would have consequences on the nondivergent kinetic energy in locations which are distant from the excess generation of P_a . Figures 3 through 6 verify this cascade during the 3 weeks prior to onset. Available potential energy is generated preferentially over the IGP in the CHEM forecast. This is a region

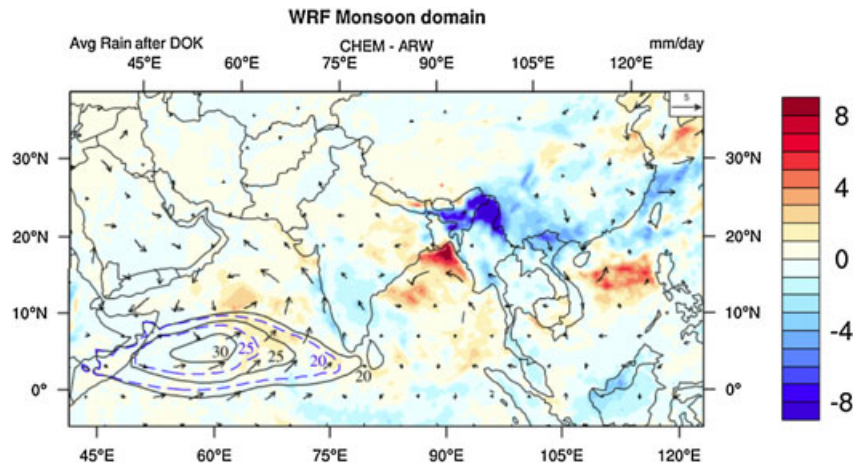


Figure 8. The difference in ensemble mean daily rainfall for the 30 days after DOK. The CHEM ensemble mean minus the NOABS ensemble mean is shown. Overlaid are the ensemble mean isotachs during the week surrounding onset for the CHEM (solid black) and NOABS (dashed blue) ensembles. Also overlaid is the anomaly (CHEM-NOABS) in ensemble mean 850 hPa flow. (m s^{-1} , black vectors).

in which there is great excess of absorbing aerosols in the CHEM forecasts. The excess generation allows more energy to be transferred to the local Hadley circulation, represented by the irrotational kinetic energy. Figure 5 shows that preferential acceleration in the CHEM irrotational circulation at 850 hPa occurs over the Himalayan foothills and over the eastern IGP near the Bengali coast. This acceleration of the irrotational circulation is a precursor to greater intensification of the AS LLJ in CHEM, which occurs nearly 2 weeks later (see Figure 7). The fact that the kinetic energy is transferred to the nondivergent flow at a location far from the IGP is confirmed by Figure 6. The end result of the excess generation of available potential energy over the IGP is a more intense and eastward displaced low-level jet, and a region of increased low-level vorticity over the western Bay of Bengal.

[47] The perturbed flow has several direct consequences on the rainfall over India during and just after onset. The daily rainfall during the month after onset was found to be quite different in the CHEM ensemble compared to NOABS. The rainfall anomaly fields suggest a SW to NE dipole in rainfall in the CHEM forecasts when compared to NOABS. The CHEM ensemble experiences as much as 2 mm day⁻¹ less rain over the southern Indian states during the early period. Conversely, the CHEM forecasts experience as much as 8 mm day⁻¹ more rain just off the coast of West Bengal and more daily rainfall throughout NE India. The CHEM ensemble also experiences diminished early season rainfall in the eastern HF. This feature is likely related to the increase in rainfall over NE India through increased low level flow curvature and diminished flow perpendicular to the Eastern Himalayas.

[48] These findings are based on a model-based sensitivity experiment. An ensemble approach was chosen in order to give some estimate of precision and significance to the ensemble mean differences. However, care should be taken attributing anything more than binary changes to the presence of aerosol absorption in CHEM. The resulting excess of midtropospheric heating can be said to intensify the AS LLJ, but how much it will intensify given a finite increment in black carbon emission over the IGP cannot be answered by this study. Also, the sensitivity of psi-chi energy exchanges to aerosol indirect effects or aerosol scattering was not explored in this study.

[49] The more intense and eastward displaced jet in the CHEM ensemble has direct consequences on the spatial pattern of rainfall over lower India. However, the amount of excess daily rainfall or of drought resulting from excess absorption by black carbon or dust cannot be accurately predicted by this methodology. More study, including intense observing periods with both chemical and meteorological sampling will be required to answer such precise questions. It is hoped that this work will illustrate that the interaction of atmospheric chemistry, radiative balance, and atmospheric fluid dynamics in the South Asian region occurs in a complex system, the character of which is changing with time. However, the mathematical tools to fully describe the system exist and can be brought to bear with the help of numerical prediction. This paper scratched the surface of the full perturbation to energy exchange which occurs as a result of highly absorptive aerosol in the monsoon region.

[50] **Acknowledgment.** NASA GSRP grant no. NNX09AL41H provided funding for this research.

References

- Abdul-Razzak, H., and S. J. Ghan (2000), A parameterization of aerosol activation 2. Multiple aerosol types, *J. Geophys. Res.*, *105*(D5), 6837–6844.
- Ackermann, I. J., H. Hass, M. Memmesheimer, A. Ebel, F. S. Binkowski, and U. Shankar (1998), Modal aerosol dynamics model for Europe: Development and first applications, *Atmos. Environ.*, *32*(17), 2981–2999, doi:10.1016/S1352-2310(98)00006-5.
- Ananthakrishnan, R., and M. K. Soman (1988), The onset of the southwest monsoon over Kerala: 1901–1980, *J. Climatol.*, *8*, 283–296.
- Babu, S. S., S. K. Satheesh, and K. K. Moorthy (2002), Aerosol radiative forcing due to enhanced black carbon at an urban site in India, *Geophys. Res. Lett.*, *29*(18), 1880, doi:10.1029/2002GL015826.
- Bollasina, M., S. Nigam, and K. M. Lau (2008), Absorbing aerosols and summer monsoon evolution over South Asia: An observational portrayal, *J. Clim.*, *21*, 3221–3229, doi:10.1175/2007JCLI2094.1.
- Bolscher, M., et al. (2007), Retro deliverable. *RETRO Documentation D1-6*.
- Chou, M.-D., and M. J. Suarez, (1999), A solar radiation parameterization for atmospheric studies, *Tech. Rep. NASA/TM-1999-104606*, NASA.
- Chung, C. E., and V. Ramanathan (2006), Weakening of north Indian SST gradients and the monsoon rainfall in India and the Sahel, *J. Clim.*, *19*, 2036–2045.
- Clough, S. A., M. W. Shephard, E. J. Mlawer, J. S. Delamere, M. J. Iacono, K. Cady-Pereira, S. Boukabara, and P. D. Brown (2005), Atmospheric radiative transfer modeling: A summary of the AER codes, *J. Quant. Spectrosc. Radiat. Transfer*, *91*, 233–244.
- Fan, F., M. E. Mann, S. Lee, and J. L. Evans (2010), Observed and modeled changes in the South Asian summer monsoon over the historical period, *J. Clim.*, *23*, 5193–5205, doi:10.1175/2010JCLI3374.1.
- Fasullo, J., and P. J. Webster (2003), A hydrological definition of Indian monsoon onset and withdrawal, *J. Clim.*, *16*, 3200–3211.
- Freud, E., D. Rosenfeld, M. O. Andrade, A. A. Costa, and P. Artaxo (2005), Robust relations between CCN and the vertical evolution of cloud drop size distribution in deep convective clouds, *Atmos. Chem. Phys. Discuss.*, *5*, 10,155–10,195.
- Freitas, S. R., K. M. Longo, M. F. Alonso, M. Pirre, V. Marecal, G. Grell, R. Stockler, R. F. Mello, and M. Sanchez Gacita (2011), PREP-CHEM-SRC - 1.0: A preprocessor of trace gas and aerosol emission fields for regional and global atmospheric chemistry models, *Geosci. Model Dev.*, *4*, 419–433, doi:10.5194/gmd-4-419-2011.
- Ginoux, P., M. Chin, I. Tegen, J. M. Prospero, B. Holben, O. Dubovik, and S.-J. Lin (2001), Sources and distributions of dust aerosols simulated with the GOCART model, *J. Geophys. Res.*, *106*, 20,255–20,273.
- Grell, G. A., S. E. Peckham, R. Schmitz, S. A. McKeen, G. Frost, W. C. Skamarock, and B. Eder (2005), Fully coupled z “online” chemistry within the WRF model, *Atmos. Environ.*, *39*(37), 6957–6975, doi:10.1029/2000JD000053.
- Grossman, R. L., and D. R. Durran (1984), Interaction of low-level flow with the Western Ghats Mountains and offshore convection in the summer monsoon, *Mon. Weather Rev.*, *112*, 652–672.
- Justice, C. O., et al. (2002), The MODIS fire products, *Remote Sens. Environ.*, *83*, 244–262, doi:10.1016/S0034-4257(02)00076-7.
- Kalnay, M. E., et al. (1996), The NCEP/NCAR 40-year reanalysis project, *Bull. Am. Meteorol. Soc.*, *77*, 437–471.
- Krishnamurti, T. N., A. Chakraborty, A. Martin, W. K. Lau, K. M. Kim, and Y. Sud (2009), Impact of Arabian Sea pollution on the Bay of Bengal winter monsoon rains, *J. Geophys. Res.*, *114*, D06213, doi:10.1029/2008JD010679.
- Krishnamurti, T. N., and V. Ramanathan (1982), Sensitivity of monsoon onset to differential heating, *J. Atmos. Sci.*, *39*, 1290–1306.
- Lacis, A. A., and M. I. Mischenko (1995), Climate forcing, climate sensitivity, and climate response: A radiative modeling perspective on atmospheric aerosols, in *Aerosol Forcing of Climate*, edited by R. Charlson, and J. Heintzenberg, pp. 11–42, John Wiley Ltd., New York.
- Lau, K. M., et al. (2008), The joint Aerosol-Monsoon experiment: A new challenge for monsoon climate research, *Bull. Am. Meteorol. Soc.*, *89*, 369–383, doi:10.1175/BAMS-89-3-369.
- Lau, K. M., M. K. Kim, and K. M. Kim (2006), Asian summer monsoon anomalies induced by aerosol direct forcing, the role of the Tibetan Plateau, *Clim. Dyn.*, *26*, 855–864, doi:10.1007/s00382-006-0114-z.
- Lelieveld, J., et al. (2001), The Indian Ocean experiment, *Science*, *291*, 1031–1036.
- Li, C., and M. Yanai (1996), The onset and interannual variability of the Asian summer monsoon in relation to land sea thermal contrast, *J. Clim.*, *9*, 1065–1092.

- Lin, Y.-L., R. D. Farley, and H. D. Orville (1983), Bulk parameterization of the snow field in a cloud model, *J. Clim. Appl. Meteorol.*, *22*, 1065–1092.
- Liu, Y., and P. H. Daum (2004), Parameterization of the autoconversion process, part 1: Analytical formulation of the Kessler-type parameterizations, *J. Atmos. Sci.*, *61*, 1539–1548.
- Mullen, S. L., and D. P. Baumhefner (1993), Monte carlo simulations of explosive cyclogenesis, *Mon. Weather Rev.*, *122*, 1548–1567.
- Ramanathan, V., and G. Carmichael (2008), Global and regional climate changes due to black carbon, *Nat. Geosci.*, *1*, 221–227, doi:10.1038/ngeo156.
- Ramanathan, V., and M. V. Ramana (2005), Persistent, widespread, and strongly absorbing haze over the Himalayan foothills and the Indo-Gangetic plains, *Pure Appl. Geophys.*, *162*, 1609–1626, doi:10.1007/s00024-005-2685-8.
- Ramanathan, V., et al. (2005), Atmospheric brown clouds: Impacts on South Asian climate and hydrological cycle, *PNAS*, *102*(15), 5326–5333.
- Ramanathan, V., et al. (2007), Atmospheric brown clouds: Hemispherical and regional variations in long-range transport, absorption, and radiative forcing, *J. Geophys. Res.*, *112*, D22S2, doi:10.1029/2006JD008124.
- Rutledge, S. A., and P. V. Hobbs (1984), The mesoscale and microscale structure and organization of clouds and precipitation in midlatitude cyclones. XII: A diagnostic modeling study of precipitation development in narrow cold-frontal rainbands, *J. Atmos. Sci.*, *41*, 2949–2972.
- Shaik, H. A., and S. J. Cleland (2008), The tropical circulation in the Australian and Asian region May to October 2007, *Aust. Met. Mag.*, *57*, 143–154.
- Skamarock, W. C., et al. (2008), A description of the Advanced Research WRF version 3. *Tech. Rep. NCAR/TN475+STR*, NCAR.
- Twomey, S. (1977), The influence of pollution on the shortwave albedo of clouds, *J. Atmos. Sci.*, *34*, 1149–1152.
- Tripathi, S. N., S. Dey, and V. Tare (2005), Aerosol black carbon radiative forcing at an industrial city in northern India, *Geophys. Res. Lett.*, *32*, L08802, doi:10.1029/2005GL022515.
- US Census Bureau (2011), International database, 10 May 2010 edition.
- Vinoj, V., S. S. Babu, S. K. Satheesth, K. K. Moorthy, and Y. J. Kaufman (2004), Radiative forcing by aerosols over the Bay of Bengal region derived from shipborne, island-based, and satellite (Moderate-Resolution Imaging Spectroradiometer) observations, *J. Geophys. Res.*, *109*, D05203, doi:10.1029/2003JD004329.
- Wang, B., Q. Ding, and P. V. Joseph (2009a), Objective definition of the Indian summer monsoon onset, *J. Clim.*, *22*, 3303–3316, doi:10.1175/2008JCLI2675.1.
- Wang, K., R. E. Dickenson, and S. Liang (2009b), Clear sky visibility has decreased over land globally from 1973 to 2007, *Science*, *232*, 1468–1470, doi:10.1126/science.1167549.
- Wu, G. X., and Y. S. Zhang (1998), Tibetan Plateau forcing and the timing of the monsoon onset over South Asia and the South China Sea, *Mon. Weather Rev.*, *126*, 913–927.
- Wu, G. X., W. P. Li, H. Guo, and H. Liu (1997), Sensible heating-driven air pump of the tibetan plateau and the asian summer monsoon, in *Memorial Volume of Prof. J. Z. Zhao*, edited by D. Z. Ye, pp. 16–126, Science Press, Beijing.